Structure Absorption Spectra Correlation in a Series of 2,6-Dimethyl-4-arylpyrylium Salts

N. Manoj,[†,§] G. Ajayakumar,[†] K. R. Gopidas,*[,†] and C. H. Suresh*[,‡]

Photosciences and Photonics Section and Computational Modelling and Simulation Section, Regional Research Laboratory (CSIR), Trivandrum 695 019, India

Received: June 21, 2006; In Final Form: August 7, 2006

A combined experimental and theoretical study of the absorption spectra of a group of closely related pyrylium perchlorates **1**−**11** are presented. Minor changes in the position of the substituents lead to drastic changes in the absorption spectra in this series of compounds. We have attempted to explain the observed changes using the *x*,*y*-band notation developed by Balaban and co-workers. Absorption spectra of all compounds are compared with results from time-dependent density functional theory (TDDFT) and Zerner's intermediate neglect of differential overlap (ZINDO/S) level calculations. Results of the calculations are in good agreement with experimental observations and an interesting correlation between Balaban's notations and the MO transitions are obtained for simple derivatives. It is suggested that for more complex systems such as α- and *β*-naphthyl substituted systems, the empirical method is not appropriate.

1. Introduction

Pyrylium salts belong to a very important class of cationic organic molecules having a trivalent oxygen atom in a six-membered aromatic ring. These molecules are of considerable theoretical and practical interest. From the theoretical standpoint, pyrylium salts represent the extreme case of a single perturbation (replacement of CH by O^+) introduced by a heteroatom into a benzene ring. Because of the positive charge, these molecules are inherently electron deficient and undergo a wide range of synthetically useful reactions.[1−4] The electron-accepting nature has also resulted in their widespread use as sensitizers for photo-induced electron transfer (PET) reactions and as photocatalysts.[5−19] The good absorption, fluorescence, and electron acceptor behavior of pyrylium salts have been exploited to design sensors for anions, amines, amino acids, and proteins.[20−27] Pyrylium salts also find applications in nonlinear optical (NLO) materials,[28−32] phototherapeutic agents,[33] and anticancer agents.[34]

For the past few years, we have been interested in the study of 2,6-dimethyl-4-arylpyrylium salts as electron-transfer sensitizers.[35,36] During the course of this study, we observed that the absorption spectra of pyrylium salts depend very much on the substitution in the 4-aryl ring. The spectral profiles and molar absorption coefficients depend not only on the nature of the substituent but also on its position of attachment. For example, the spectral profiles change drastically if a substituent is shifted from the para to the ortho or meta position. Absorption spectral characteristics of pyrylium salts are extremely important in the design of sensors, phototherapeutic agents, or NLO materials based on pyrylium salts. Hence, we undertook an experimental and theoretical study of the absorption spectral properties of simple pyrylium salts. In this paper, absorption spectra of 11 2,6-dimethyl-4-arylpyrylium salts (**1**−**11** in Chart 1) are presented. These compounds are compiled into four groups and their spectra are analyzed in the light of earlier empirical studies. Absorption spectra of **1**−**11** were also obtained using TDDFT/B3LYP/6-31G* and ZINDO/S level calculations. We observed good agreement in the assignments made on the basis of empirical results and theoretical calculations.

CHART 1: Structures of the Pyrylium Salts

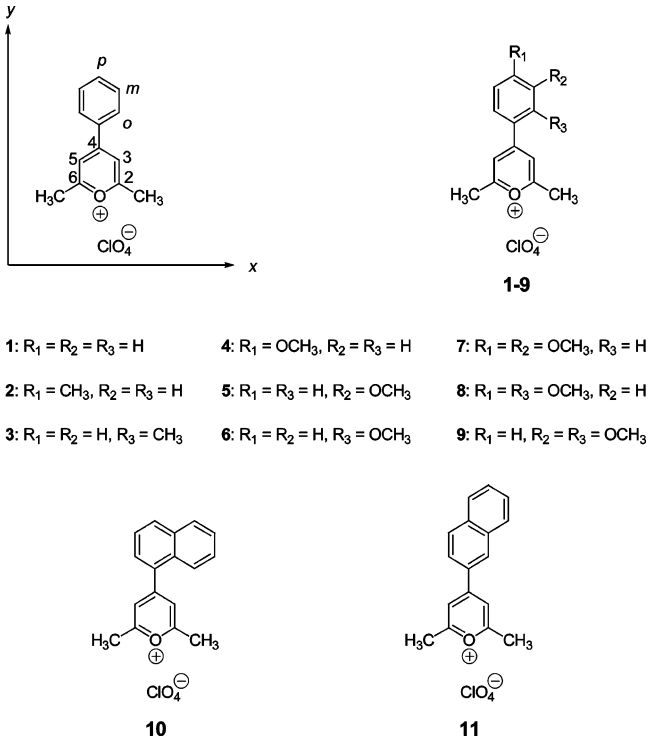

2. Experimental Section

The synthesis of some of the pyrylium salts was reported in our earlier papers.[35,36] Other derivatives were prepared using the same general procedure. These were fully characterized by spectroscopic methods and elemental analysis. Absorption spectra were recorded using a Shimadzu UV 3101 PC UV−vis

* Author to whom correspondence should be addressed. Phone: 91-471-2515364; e-mail: gopidaskr@rediffmail.com and sureshch@gmail.com.
† Photosciences and Photonics Section.
‡ Computation and Modelling Section.
§ Present address: Lehrstuhl Umweltmesstechnik, University of Karlsruhe, Germany.

10.1021/jp063867d CCC: $33.50
Published on Web 09/12/2006

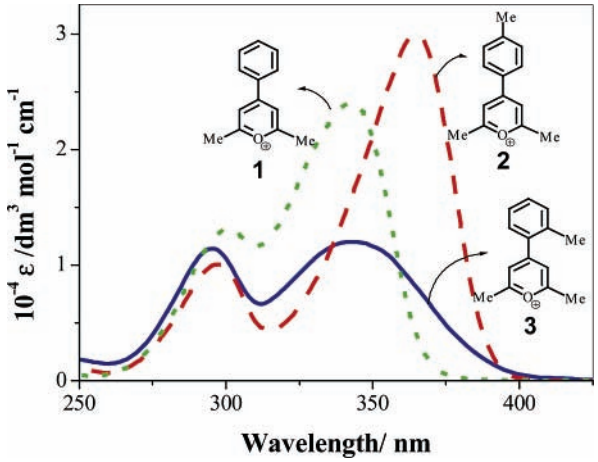

Figure 1. Absorption spectra of **1**−**3** in dichloromethane solution.

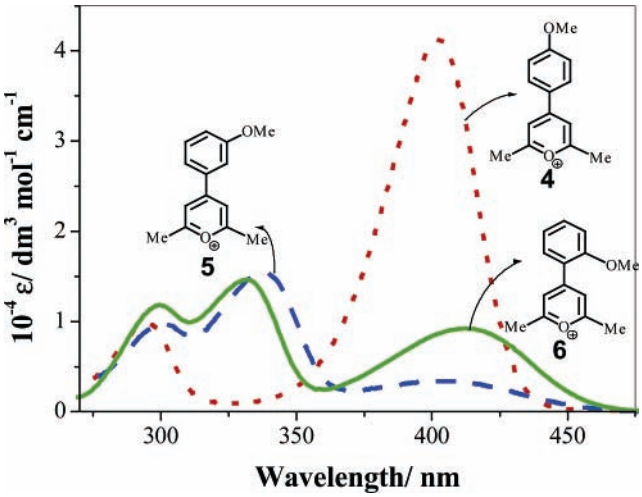

Figure 2. Absorption spectra of **4**−**6** in dichloromethane.

spectrometer. Spectroscopic grade dichloromethane and acetonitrile were used for the studies.

3. Results and Discussion

3.1. Absorption Spectra. Absorption spectra of pyrylium salts **1**−**3** in dichloromethane are presented in Figure 1. When the 4-phenyl ring is unsubstituted as in **1**, a broad absorption with maximum at 343 nm was observed. When the 4-phenyl ring is substituted with a methyl group at the para position, the molar absorption coefficient increases with a decrease in the full width at half-maximum (fwhm) value. When the methyl substitution is in the ortho position as in **3**, the molar absorption coefficient decreases considerably with an increase in the fwhm value.

Pyrylium salts **4**−**6** differ only by the position (para, meta, or ortho) of the methoxy substituent in the 4-phenyl ring. Absorption spectra of these compounds exhibited pronounced differences as shown in Figure 2. Compound **4** exhibited a very intense band around 402 nm. In the case of **5** and **6**, the band around 400 nm is weak, but they exhibited an additional moderately strong band around 330−340 nm.

Dimethoxy derivatives **7**−**9** also exhibit markedly different absorption spectra (Figure 3). In the case of **7** and **8**, the long wavelength absorption above 400 nm is very intense and the absorption around 355 nm is very weak. The trend is reversed for **9**.

Absorption spectra of 4-aryl derivatives **10** and **11** in dichloromethane are shown in Figure 4. The α-naphthyl

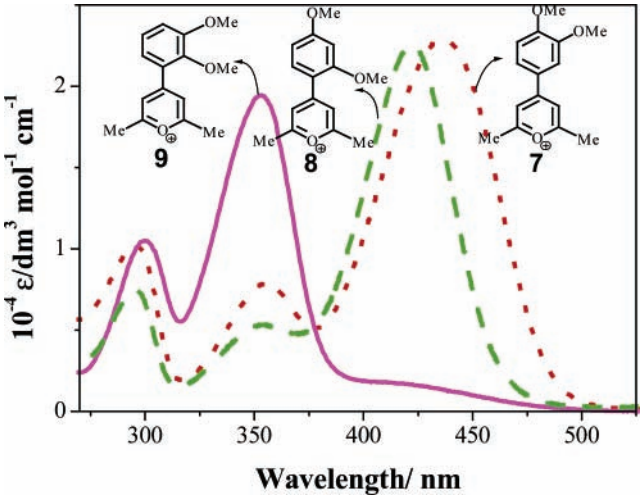

Figure 3. Absorption spectra of **7**−**9** in dichloromethane.

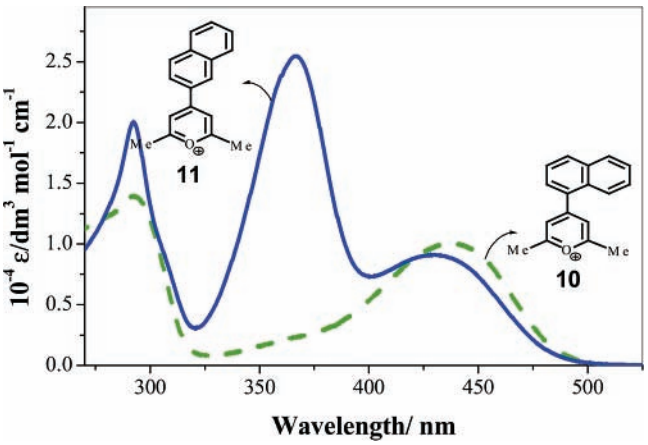

Figure 4. Absorption spectra of **10** and **11** in dichloromethane solution.

substituted derivative **10** exhibits a moderately strong band at 438 nm. The β-naphthyl substituted derivative **11** on the other hand exhibited two bands in the 350−500 nm region.

As seen in Figures 1−4, all pyrylium salts studied exhibit short wavelength absorption at 300 nm and one or two absorption bands in the 330−430 nm region. When the solvent was changed to acetonitrile, the 300 nm band remained unaffected in all cases, but the long wavelength absorptions exhibited a 20−30 nm blue shift with a slight decrease in the molar absorption coefficient. For example, in acetonitrile the absorption band of **1** is blue shifted to 326 nm compared to 343 nm in dichloromethane. In general, pyrylium salts exhibit blue shifts in polar solvents, and this is attributed to the better stabilization of the polar ground state compared to the excited state in polar solvents.

Why is it that positional isomers such as **2**−**3**, **4**−**6**, **7**−**9**, or **10**−**11** exhibit markedly different absorption spectra? To answer this question, we have taken a close look at the literature reports regarding the absorption spectra of pyrylium salts. Several spectroscopic studies, both experimental and theoretical, have been carried out on pyrylium salts and their structural analogues.[37−43] Balaban and co-workers, for example, correlated the absorption bands in simple pyrylium systems to those in benzene, pyridine, and pyridinium salts. Absorption bands in the pyrylium systems were designated as "*x*" bands and "*y*" bands, depending on the direction of polarization of these bands.[1] The effect of substituents in the ring on the absorption bands was also studied. It was observed that substituents in the 2- and 6-positions affect the *x*-band and substituents in the

4-position affect the *y*-band predominantly (see Chart 1 for axes notation). These observations were in agreement with the projections of the substituents in the *x* and *y* axes. Thus in **1**, the 300 nm band was assigned as the *x*-band and the 326 nm band (in acetonitrile) as the *y*-band. Balaban and co-workers later suggested that the 326 nm band in **1** is a superposition of two closely lying bands, namely, the weak $S_0 \rightarrow S_1$ band (calculated λ_{max} in acetonitrile = 334 nm, polarized along the *x*-axis, *x*-band) and the strong $S_0 \rightarrow S_2$ band (calculated λ_{max} in acetonitrile = 325 nm, polarized along the *y*-axis, *y*-band).[40] The band separation is very small (9 nm, corresponds to $\Delta E = 825\ cm^{-1}$), and hence these bands are not resolved. The fwhm is high for this band (Figure 1) suggesting that this band indeed is a superposition of two absorption bands.

Balaban's *x*- and *y*-band notation can be extended to explain the absorption spectra of pyrylium salts **1**−**11.** The 4-phenyl ring and para-substituted 4-phenyl rings can be considered as pure *y*-substituents. These compounds are characterized by one strong absorption at ≥350 nm region. If the substituents are in the ortho or meta positions of the 4-phenyl ring, contributions due to the substituents can be projected into the *x*- and *y*-directions. As a result, these systems will exhibit two absorption bands in the ≥350 nm region. The *o*-methyl substituted derivative **3** and the α-naphthyl substituted derivative **10** appear to be exceptions. However, the absorption bands in these cases are very broad, and this may be due to superposition of close-lying *x*- and *y*-bands. To obtain a theoretical explanation of the band notation, we attempted theoretical calculations on these molecules, and the results are summarized in the next section.

3.2. Theoretical Modeling. *3.2.1. Methods.* Density functional theory (DFT) methods have been accepted as efficient and reasonably accurate methods, and they have become a powerful tool in molecular modeling, particularly for the ground-state properties.[44,45] In the present work, all the ground-state geometries have been optimized at DFT level by using the Becke's three-parameter exchange functional[46] in conjunction with the Lee−Yang−Parr correlation functional[47] as implemented in the Gaussian 03 suite of programs.[48] For all the atoms, the 6-31G(d) basis functions were selected. This DFT method known as B3LYP/6-31G(d) is one of the most widely used methods for getting a very good structural description of molecular systems. All the optimized structures were confirmed as energy minima by normal coordinate analysis. The basic photochemical properties of these systems have been investigated by means of quantum chemical calculations employing mainly the TDDFT/B3LYP/6-31G* formalism[49−51] as well as ZINDO/S method.[52] Both these methods are best suited for the computation of low-lying valence excited states, and they have been successfully applied for a wide variety of problems.[53−58]

3.2.2. Optimized Geometries and Electronic Properties of Pyrylium Systems. Optimized structures of all the systems are depicted in Figure 5 along with some important geometrical parameters. The first noticeable structural feature is the twist angle (θ) between the pyrylium and 4-phenyl rings. The unsubstituted derivative **1** shows θ value of 28.4°. The θ value is the smallest (16.8°) for the dimethoxy derivative **7** and the largest (39.3°) for the α-naphthyl derivative **11**. Large θ values are observed when an ortho substituent is present in the phenyl ring (e.g., **3**, **6**, **9**, and **10**) suggesting significant steric effects, while relatively small θ values are observed in the para-substituted systems (**2**, **4**, **7**, and **8**). The bond length parameters shown in Figure 5 indicate that a para substituent is more strongly bonded to the phenyl ring than the meta, and the latter is more strongly bonded to the ring than the ortho substituent. For instance, the C−OMe bond lengths in **4** (*p*-OMe), **5** (*m*-OMe), and **6** (*o*-OMe) are 1.335, 1.349, and 1.351 Å, respectively. Similarly, the $C-CH_3$ bond distance of 1.503 Å in **2** (*p*-Me) is smaller than the corresponding distance of 1.513 Å found in **3** (*o*-Me). The shorter value found in the para-substituted systems points toward strong mesomeric interaction between the lone pair on OCH_3 oxygen and the arene ring π-system and strong inductive electron donation from CH_3 substituent.

To understand the electronic effects of the substituents, we have also analyzed the Mulliken charge on these systems. In Figure 5, the charges on the pyrylium and the phenyl rings are presented (inside the rings). In the case of the unsubstituted system **1**, the charges on the pyrylium and phenyl rings are 0.72 and 0.28, respectively. All substituents we have employed are electron donating in nature, and the substitutions have resulted in lowering of charge on the pyrylium ring and increasing of charge on the 4-phenyl ring (Figure 5). An electron-donating group is most effective in the ortho−para orientation and is less effective in the meta orientation. In the present case, however, ortho substitution leads to steric crowding and results in nonplanarity and reduction in conjugation. Thus, the effect of substituents in the present case is expected to be para > meta > ortho. In light of this, we find that there is excellent agreement between the substituent effect, calculated θ values, and Mulliken charges and observed absorption maxima for the systems studied. As we can see, the electron-donating substituent at the para position decreases the charge on the pyrylium ring to the maximum extent as compared to the substituent at other positions. The para-substituted systems are also more planar and show small θ values. Thus, conjugation effects will be more in the para-substituted systems. In the case of disubstituted systems, effect of the para substitution is more prominent. For instance, the θ value for disubstituted system **8** (*o*,*p*-di-OMe**)** is smaller than that of the monosubstituted system **6** (*o*-OMe).

We have also found a correlation between the Mulliken charge on the pyrylium ring and the λ_{max} values. In Figure 6, we have plotted the Mulliken charges against the λ_{max} values of the most intense absorptions of **1**−**11**. It can be seen that the correlation is very good except for the α-naphthyl system **11.** The decrease in the positive charge on the pyrylium ring is directly related to the enhancement in the π-conjugation via the inductive and mesomeric effect of the substituents. This in turn will reduce the energy gap between the frontier molecular orbitals, and therefore higher wavelength absorption is expected in systems with lower positive charge on the pyrylium ring.

3.2.3. TDDFT and ZINDO Calculations. In Tables1 and 2, the TDDFT and ZINDO results are summarized along with the experimental values of the λ_{max} and the corresponding molar absorption coefficients. In general, the theoretical absorption maxima (λ_{max}) obtained by the two methods for the pyrylium systems are in good agreement with the corresponding experimental values (in CH_2Cl_2). The only exceptions are the longer wavelength absorptions calculated for **5** (*m*-OMe**)**, **9** (*o*,*m*-di-OMe), **10** (α-naphthyl), and **11** (β-naphthyl) systems at the TDDFT level, which showed a significant deviation from the experimental λ_{max}. On the other hand, λ_{max} values calculated at the ZINDO level showed good agreement with all the experimental λ_{max} values. In Tables 1 and 2, the MO transitions corresponding to the absorption peaks and their contributions are also listed. Inspection of molecular orbital (MO) transitions reveals that for the unsubstituted system **1** and all the para-substituted systems (singly and doubly substituted systems), the

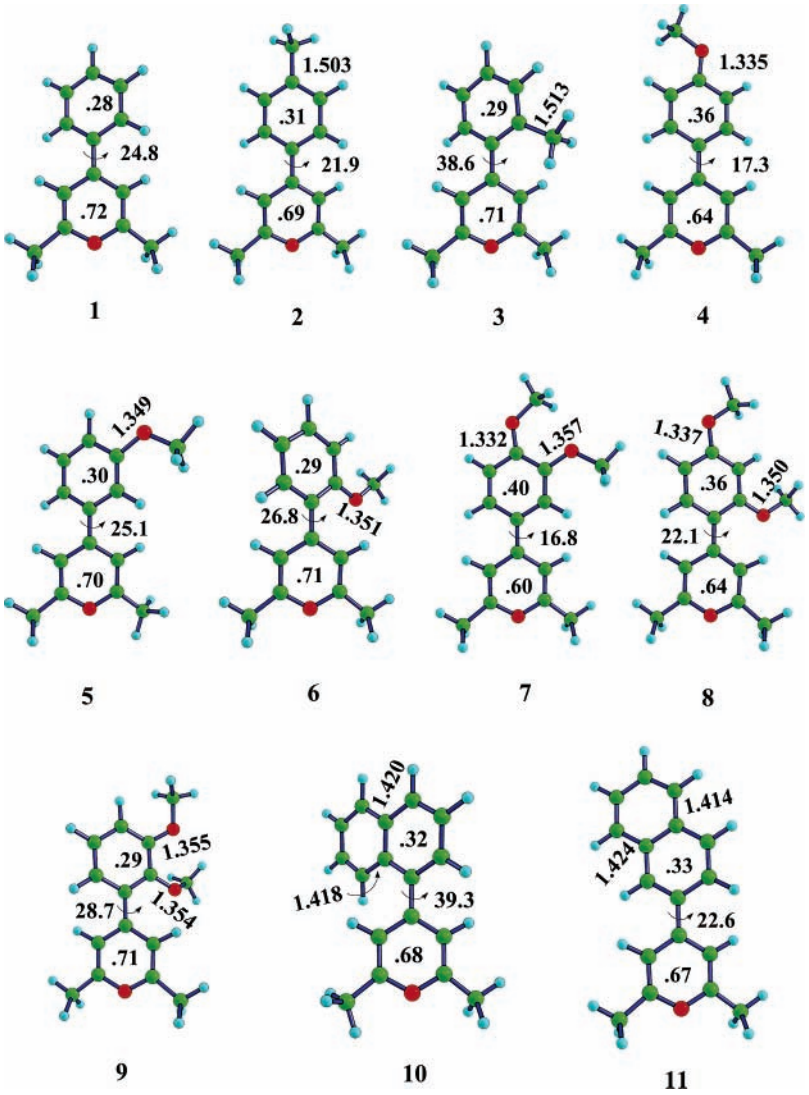

Figure 5. B3LYP/6-31G(d,p) level optimized geometry of pyrylium systems showing some important geometry parameters and the Mulliken charges (indicated inside the rings). Bond lengths are in angstroms and twist angles are in degrees.

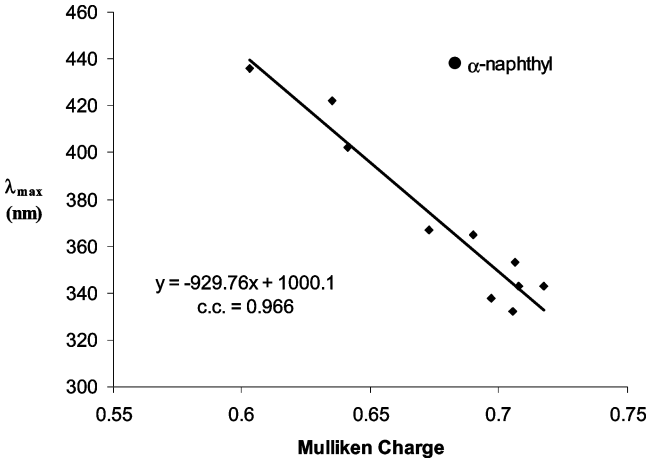

Figure 6. Correlation between the λ_{max} and Mulliken charge on the pyrylium ring.

prominent electron transitions from highest occupied molecular orbital (HOMO) to lowest unoccupied molecular orbital (LUMO), whereas in the case of systems containing no para substitution (meta, ortho, and ortho−meta substituted systems), the main absorption peak originates from a HOMO-1 to LUMO electron transition. In the case of **10** (α-naphthyl), the theory and experiment suggest only one absorption peak which corresponds to the HOMO to LUMO transition while in the case of **11** (*β*-naphthyl), two absorption peaks are detected wherein the main peak corresponds to the HOMO-1 to LUMO transition.

In Figure 7, the HOMO-1, HOMO, and LUMO (obtained from TDDFT/B3LYP/6-31G* method) of pyrylium salt **2** are given along with the axis notation. The *y*-axis is considered as passing through the C−C bond that connects the pyrylium ring to the 4-phenyl ring. For all the pyrylium salt systems studied herein, the HOMO and HOMO-1 are mainly localized on the phenyl ring while the LUMO is mainly centered on the pyrylium ring. Therefore, it is clear that irrespective of the substituent in the system, the electronic excitation in the 4-arylpyrylium salts always leads to the transfer of electron from the 4-phenyl ring to the electron deficient pyrylium ring along the *y*-direction.

In the unsubstituted system **1** and all the systems with single para substitution (**2** and **4**), the HOMO-1, HOMO, and LUMO have features as shown in Figure 7. As we can see, the HOMO-1 has its entire electron density localized on the 4-phenyl ring and possesses a nodal plane along the *y*-axis. The HOMO is mainly localized on the phenyl ring and it has a nodal plane in the *x*-axis, whereas the LUMO is largely centered on the pyrylium ring. Pyrylium salts **1**, **2**, and **4** exhibited a very strong absorption at ≥350 nm ($\epsilon > 2.5 \times 10^4$ dm^3 mol^{-1} cm^{-1}), which

TABLE 1: Calculated TDDFT Excitation Energies, MO Contributions, and Oscillator Strengths along with Experimental Values

system	TDDFT theor. λ_{max} (nm)	HOMO & HOMO-1 to LUMO transition and % contribution of: HOMO	HOMO-1	expt. λ_{max} (nm) in CH_2Cl_2	TDDFT osc. strength	expt. molar abs. coeff (10^4 dm^3 mol^{-1}cm^{-1})
1	342	63	0	343 (*y*)	0.4843	2.4
2 (*p*-Me)	359	63	0	365 (*y*)	0.6002	3.0
3 (*o*-Me)	363	13	63	343 (*x*)	0.3577	1.2
4 (*p*-OMe)	381	61	0	402 (*y*)	0.6861	4.1
5 (*m*-OMe)	523	65	15	405 (*x*)	0.0497	0.3
	354	10	63	338 (*y*)	0.3558	1.5
6 (*o*-OMe)	452	65	16	412 (*x*)	0.0981	0.9
	336	11	64	332 (*y*)	0.3881	1.5
7 (*p*,*m*-di-OMe)	453	57	27	436 (*y*)	0.3247	2.3
	371	20	62	355 (*x*)	0.3626	0.8
8 (*o*,*p*-di-OMe)	407	56	33	417 (*y*)	0.3107	1.9
	357	27	59	353 (*x*)	0.3801	0.2
9 (*o*,*m*-di-OMe)	571	68	0	422 (*x*)	0.0155	0.5
	371	0	64	355 (*y*)	0.3737	2.2
10 (α-naphthyl)	509	64	0	438 (*y*)	0.2076	1.0
11 (*β*-naphthyl)	544	64	19	430 (*x*)	0.0772	0.9
	391	13	62	367 (*y*)	0.4991	2.5

TABLE 2: Calculated ZINDO Excitation Energies, MO Contributions, and Oscillator Strengths along with Experimental Values

system	ZINDO theor. λ_{max} (nm)	HOMO & HOMO-1 to LUMO transition and % contribution of: HOMO	HOMO-1	expt. λ_{max} (nm) in CH_2Cl_2	ZINDO osc. strength	expt. molar abs. coeff (10^4 dm^3 mol^{-1}cm^{1})
1	353	69	0	343 (*y*)	0.6692	2.4
2 (*p*-Me)	374	68	0	365 (*y*)	0.7642	3.0
3 (*o*-Me)	339	17	65	343 (*x*)	0.1297	1.2
4 (*p*-OMe)	394	68	0	402 (*y*)	0.8715	4.1
5 (*m*-OMe)	389	68	0	405 (*x*)	0.2911	0.3
	344	0	67	338 (*y*)	0.3316	1.5
6 (*o*-OMe)	389	68	0	412 (*x*)	0.4103	0.9
	330	0	66	332 (*y*)	0.2473	1.5
7 (*p*,*m*-di-OMe)	422	68	0	436 (*y*)	0.7914	2.3
	347	0	65	355 (*x*)	0.0821	0.8
8 (*o*,*p*-di-OMe)	406	68	0	417 (*y*)	0.7143	1.9
	333	0	64	353 (*x*)	0.1125	0.2
9 (*o*,*m*-di-OMe)	404	65	20	422 (*x*)	0.1077	0.5
	360	19	65	355 (*y*)	0.5147	2.2
10 (α-naphthyl)	466	68	0	438 (*y*)	0.4352	1.0
11 (*β*-naphthyl)	445	67	11[a]	430 (*x*)	0.3911	0.9
	376	0	65	367 (*y*)	0.4433	2.5

[a] At ZINDO level, this orbital was HOMO-2.

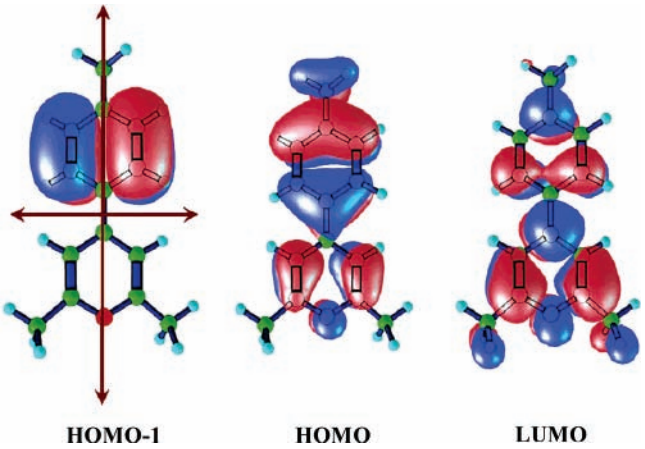

Figure 7. HOMO-1, HOMO, and LUMO orbitals of **2**.

we assign to the HOMO → LUMO transition (Tables 1 and 2). A transition corresponding to HOMO-1 → LUMO is not observed. Therefore, it is quite clear that electron transition from the orbital having a nodal plane passing through the *y*-axis (HOMO-1, in this case) is not allowed while that from the orbital with a nodal plane in the *x*-direction (HOMO in this case) is strongly allowed. Thus, the λ_{max} observed for **1**, **2**, and **4** can be grouped into the same class, which arises from the HOMO → LUMO transition. We propose that this transition is synonymous with Balaban's *y*-band notation. Balaban's *x*-band would then correspond to the HOMO-1 → LUMO transition (for **1**, **2**, and **4**). In the case of **1**, **2**, and **4**, the *x*-band is very weak or absent.

HOMO-1, HOMO, and LUMO for the dimethoxy derivatives **7** (*p*,*m*-di-OMe) and **8** (*o*,*p*-di-OMe) are given in Figure 8. For these systems, the nodal plane properties of HOMO-1 and HOMO are not exactly in the *y*- or *x*-axes (the nodal plane of HOMO-1 is close to the *y*-axis and the nodal plane of HOMO is close to the *x*-axis), and therefore electronic transitions from both the orbitals are expected. The orbital picture suggests a strong HOMO → LUMO transition and a weak HOMO-1 → LUMO transition. This is in agreement with the two peaks observed experimentally for these systems. Except for the nodal plane, the HOMO-1 of **7** and **8** closely resembles the HOMO-1 of **1**, **2**, and **4**. HOMO of **7** and **8** similarly retains most of the features of the HOMO of **1**, **2**, and **4** also. Thus, in **7** and **8** also, the lowest energy (HOMO → LUMO) transition is

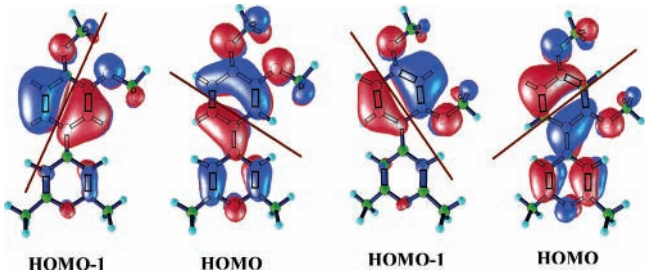

Figure 8. HOMO-1 and HOMO orbitals of **7** (*p*,*m*-di-OMe) and **8** (*o*,*p*-di-OMe) systems.

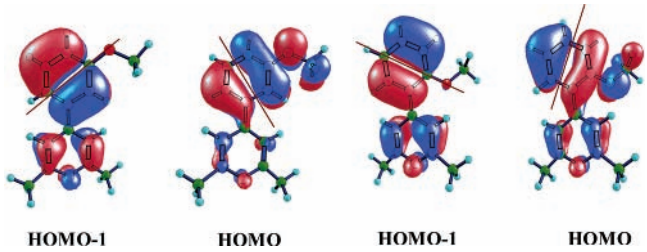

Figure 9. HOMO-1 and HOMO orbitals of **5** (*m*-OMe) and **6** (*o*-OMe) systems.

assigned to the *y*-band. The weak band around 350 nm is attributed to the HOMO-1 → LUMO transition, and this is assigned as the *x*-band.

For the systems we have described so far (**1**, **2**, **4**, **7**, and **8**), the long wavelength absorption is assigned as the *y*-band. For these systems, the HOMO-1 orbitals have their nodal plane close to the *y*-axis and the HOMO orbitals have their nodal planes close to the *x*-axis. The situation is reversed for the ortho- and meta-substituted derivatives **3**, **5**, and **6**. In Figure 9, the HOMO-1 and HOMO of **5** (*m*-OMe) and **6** (*o*-OMe) are given. For **5** and **6**, the HOMO-1s have their nodal planes nearly in the *x*-axis and the HOMOs have their nodal planes nearly in the *y*-axis. Also, in **1**, **2**, **4**, **7**, and **8**, the HOMO-1 orbitals have practically no electron density in the pyrylium ring. In the case of **5** and **6**, the HOMO-1 orbitals have significant electron density in the pyrylium ring. For the latter group of molecules, the HOMO orbitals have very little electron density in the pyrylium ring. Therefore, we propose that a reversal of the orbital ordering is taking place in **5** and **6**, compared to **1**, **2**, **4**, **7**, and **8**. Thus, the HOMO → LUMO transition in **5** and **6** corresponds to the *x*-band and the HOMO-1 → LUMO transition corresponds to the *y*-band. In other words, the lowest energy band in **5** and **6** are the *x*-bands (and not *y*-bands as seen in the case of **1**, **2**, **4**, **7**, and **8**).

Orbital features of **3** are found to be very similar to those of **5.** Therefore, both HOMO-1 → LUMO (*y*-band) and HOMO → LUMO (*x*-band) transitions are allowed in **3**. However, we observed only one band in the 350 nm region for **3**. The fwhm for this band is very large, and we suggest that the observed band is a superposition of the *x*- and *y*-bands, with the *x*-band at lower energy.

The HOMO-1 and HOMO orbitals of the *o*,*m*-dimethoxy derivative **9** is shown in Figure 10. A comparison with the orbitals of **7** and **8** (Figure 8) shows that a reversal of orbital ordering is taking place in the case of **9**. The HOMO of **9** with a nodal plane close to the *y*-axis and no electron density in the pyrylium ring resembles the HOMO-1s of **7** and **8**. Similarly, the HOMO-1 of **9** with the nodal plane close to the *x*-axis resembles the HOMOs of **7** and **8**. Thus, as in the case of **5** and **6**, in **9** the HOMO → LUMO transition corresponds to the *x*-band and the HOMO-1 → LUMO transition corresponds to the *y*-band.

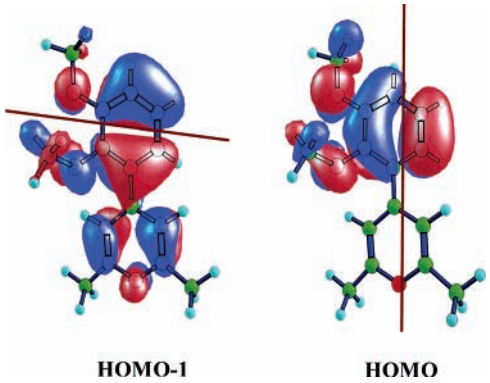

Figure 10. HOMO-1 and HOMO orbitals of **9**.

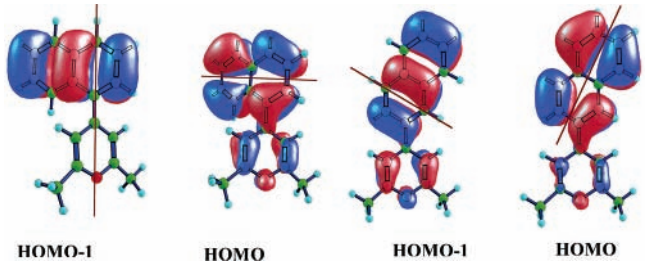

Figure 11. HOMO-1 and HOMO orbitals of **10** (α-naphthyl) and **11** (*β*-naphthyl).

In the case of α-naphthyl derivative **10**, the HOMO shows the nodal plane nearly in the *x*-direction while the HOMO-1 has its nodal plane in the *y*-direction. The situation is similar to those observed for the para-substituted derivatives **1**, **2**, and **4**. Compound **10** exhibited only one band (as in the case of **1**, **2**, and **4**), and this can be assigned as the *y*-band. In the case of the *β*-naphthyl system **11**, the nodal plane of HOMO-1 was close to the *x*-direction, and the nodal plane of HOMO was close to the *y*-direction. This picture is close to those in **5**, **6**, and **9**. Thus, we expect two bands for **11**, the weak, longer wavelength band assigned to the *x*-band and the strong, short-wavelength band assigned to the *y*-band. This result is in good agreement with experiment.

According to Balaban's notation, para substitution would lead to a red shift in the *y*-band, and ortho and meta substitution would lead to a red shift in the *x*-band. Thus, the lowest energy band in para-substituted derivatives is the *y*-band. In the case of ortho- and meta-substituted derivatives, the lowest energy band will be the *x*-band. It is very interesting to note that a good correlation exists between Balaban's *x*,*y*-band notation and the transitions predicted on the basis of calculated molecular orbital picture for the methyl- and methoxy-substituted derivatives **1**−**9**, and this is shown in Scheme 1. In the case of para-substituted derivatives (**1**, **2**, **4**, **7**, and **8**), the HOMO → LUMO transition can be assigned as the *y*-band and the forbidden HOMO-1 → LUMO transition can be assigned as the *x*-band (vide supra). In the case of ortho- and meta-substituted derivatives (**3**, **5**, **6**, and **9**), the *x*-band undergoes red shift and corresponds to the HOMO → LUMO transition. In these cases, the *y*-band corresponds to HOMO-1 → LUMO transition. In all cases, transitions corresponding to the *y*-band are more intense. It appears that this simple correlation is sufficient to assign the absorption bands in the series of pyrylium salts **1**−**9**. The *x*,*y* notations for all compounds studied are given in Tables 1 and 2.

The correlation, however, breaks down for complex derivatives such as the α- and *β*-naphthyl substituted systems **10** and **11**: α-naphthyl substitution is equivalent to ortho,meta-di-

SCHEME 1

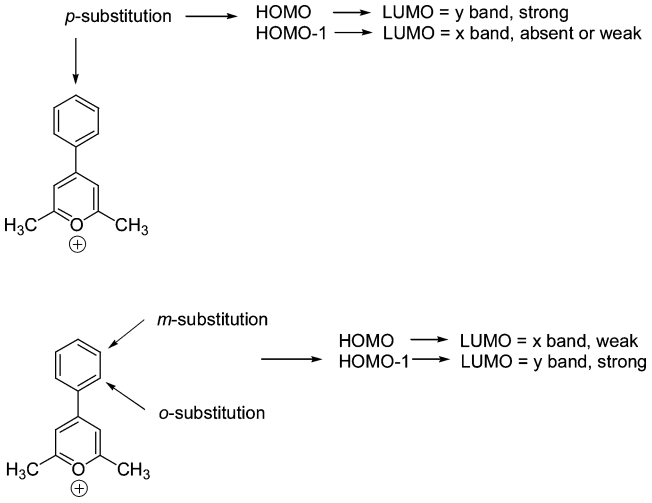

substitution, and according to Balaban's notation we expect two bands, with a red-shifted *x*-band. Experimentally, we observe only one band and this is assigned to the *y*-band (vide supra) from the orbital picture. The β-naphthyl derivative **11** can be considered as a para,meta-di-substituted derivative similar to **7**. According to the *x*,*y*-notation, one can anticipate two bands with the lower energy *y*-band more intense than the *x*-band. Two bands are actually observed experimentally, but the lowest energy band is the weak one and the orbital picture suggested that this corresponds to the *x*-band. We conclude that the simple *x*,*y*-notation is very useful for simple substituents such as alkyl or alkoxy but is not useful when the substitution pattern is more complicated. It is expected that the calculations and the empirical correlations will help greatly in the design of pyrylium salts with useful absorption properties.

4. Conclusions

Absorption spectra of a series of 4-phenyl-2,6-dimethylpyrylium salts are studied. The absorption spectra are highly sensitive to the position of substituents in the 4-phenyl ring. DFT and ZINDO calculations were carried out to explain the observed spectra. Results of the calculations are in good agreement with the experimental results. Moreover, we found that, for alkyl- and alkoxy-substituted derivatives, an empirical method used earlier to explain the absorption spectra in pyrylium salts is adequate to explain the spectra, and this empirical method can be correlated very well to the theoretical results. For more complex systems such as α- and β-naphthyl substituted systems, this empirical method breaks down. In all cases, the observed absorption spectra are very well explained by the calculated molecular orbital picture.

Acknowledgment. The authors thank the Council of Scientific and Industrial Research (CSIR) and the Department of Science and Technology (DST), Government of India, for financial support. This is contribution No. PPD(PRU)-RRLT 121 from the Photosciences and Photonics group.

References and Notes

(1) Balaban, A. T.; Fischer, G. W.; Dinculescu, A.; Koblik, A. V.; Dorofeenko, G. N.; Mezheritskii, V. V.; Schroth, W. *Pyrylium Salts: Synthesis, Reactions and Physical Properties*; Advances in Heterocyclic Chemistry, Supplement 2; Katrisky, A. R., Ed.; Academic Press: New York, 1982.

(2) Balaban, A. T.; Gavat, M.; Frangopol, P. T.; Mocanu, M.; Nenitzescu, C. D. *Rev. Roum. Chim.* **1964**, *9*, 79.

(3) Balaban, T. S.; Balaban, A. T. In *Science of Synthesis*; *Houben-Weyl Methods of Molecular Transformations*; Thomas, D. E., Ed.; Georg Thieme Verlag: Stuttgart, Germany, Vol. 14, 2003; pp 11−200.

(4) Balaban, A. T. In *Encyclopaedia of Reagents for Organic Synthesis*; Paquette, L. A., Ed.; Wiley: New York; Vol. 8, 1995; pp 5407−5411.

(5) Che, Y.; Ma, W.; Ji, H.; Zhao, J.; Ling, Z. *J. Phys. Chem. B* **2006**, *110*, 2942.

(6) Latour, V.; Pigot, T.; Simon, M.; Cardy, H.; Lacombe, S. *Photochem. Photobiol. Sci.* **2005**, *4*, 221.

(7) Halder, M. *Chem. Phys.* **2004**, *303*, 243.

(8) Miranda, M. A.; Izquierdo, M. A.; Perez-Ruiz, R. *J. Phys. Chem. A* **2003**, *107*, 2478.

(9) Miranda, M. A.; Izquierdo, M. A. *Photochem. Photobiol. Sci.* **2003**, *2*, 848.

(10) Miranda, M. A.; Izquierdo, M. A.; Galindo, F. *J. Org. Chem.* **2002**, *67*, 4138.

(11) Miranda, M. A.; Izquierdo, M. A.; Galindo, F. *Org. Lett.* **2001**, *3*, 1965.

(12) Sanjuan, A.; Pillai, M. N.; Alvaro, M.; Garcia, H. *Chem. Phys. Lett.* **2001**, *341*, 153.

(13) Khairutdinov, R. F.; Hurst, J. K. *J. Am. Chem. Soc.* **2001**, *123*, 7352.

(14) Miranda, M. A.; Garcia, H. *Chem. Rev.* **1994**, *94*, 1063.

(15) Amat, A. M.; Arques, A.; Bossmann, S. H.; Braun, A. M.; Miranda, M. A.; Vercher, R. F. *Catal. Today* **2005**, *101*, 383.

(16) Amat, A. M.; Arques, A.; Bossmann, S. H.; Braun, A. M.; Goeb, S.; Miranda, M. A.; Oliveros, E. *Chemosphere* **2004**, *57*, 1123.

(17) Alvaro, M.; Carbonell, E.; Fornes, V.; Garcia, H. *New J. Chem.* **2004**, *28*, 631.

(18) Haberl, U.; Steckhan, E.; Blechert, S.; Wiest, O. *Chem. Eur. J.* **1999**, 5, 2859.

(19) Khairutdinov, R. F.; Hurst, J. K. *Nature* **1999**, *402*, 509.

(20) Garcia-Acosta, B.; Comes, M.; Bricks, J. L.; Kudinova, M. A.; Kurdyukov, V. V.; Tolmachev, A. I.; Descalzo, A. B.; Marcos, M. D.; Martinez-Manez, R.; Moreno, A.; Sancenon, F.; Soto, J.; Villaescusa, L. A.; Rurack, K.; Barat, J. M.; Escriche, I.; Amoros, P. *Chem. Commun.* **2006**, 2239.

(21) Chernova, R. K.; Yastrebova, N. I.; Ivanova, M. A. *J. Anal. Chem.* **2006**, *61*, 230.

(22) Comes, M.; Marcos, M. D.; Martinez-Manez, R.; Millan, M. C.; Ros-Lis, J. V.; Sancenon, F.; Soto, J.; Villaescusa, L. A. *Chem. Eur. J.* **2006**, *12*, 2162.

(23) Garcia, F.; Garcia, J. M.; Garcia-Acosta, B.; Martinez-Manez, R.; Sancenon, F.; Soto, J. *Chem. Commun.* **2005**, 2790.

(24) Comes, M.; Marcos, M. D.; Martinez-Manez, R.; Sancenon, F.; Soto, J.; Villaescusa, L. A.; Amoros, P.; Beltran, D. *Adv. Mater.* **2004**, *16*, 1783.

(25) Jimenez, D.; Martinez-Manez, R.; Sancenon, F.; Ros-Lis, J. V.; Benito, A.; Soto, J. *J. Am. Chem. Soc.* **2003**, *125*, 9000.

(26) Wetzl, B. K.; Yarmoluk, S. M.; Craig, D. B.; Wolfbeis, O. S. *Angew. Chem., Int. Ed.* **2004**, *43*, 5400.

(27) Moghimi, A.; Maddah, B.; Yari, A.; Shamsipur, M.; Boostani, M.; Fall Rastegar, M.; Ghaderi, A. R. *J. Mol. Struct.* **2005**, *752*, 68.

(28) Alvaro, M.; Aprile, C.; Benitez, M.; Bourdelande, J. L.; Garcia, H.; Herance, J. R. *Chem. Phys. Lett.* **2005**, *414*, 66.

(29) Purvinis, G.; Priambodo, P. S.; Pomerantz, M.; Zhou, M.; Maldonado, T. A.; Magnusson, R. *Opt. Lett.* **2004**, *29*, 1108.

(30) Polysoz, I.; Tsigaridas, G.; Fakis, M.; Giannetas, V.; Persephonis, P.; Mikroyannidis, J. *Chem. Phys. Lett.* **2003**, *369*, 264.

(31) Zhou, Y.-F.; Feng, S.-Y. *ChemPhysChem* **2002**, *3*, 969.

(32) Fakis, M.; Tsigaridas, G.; Polyzos, I.; Giannetas, V.; Persephonis, P.; Spiliopoulos, I.; Mikroyannidis, J. *Chem. Phys. Lett.* **2001**, *342*, 155.

(33) Detty, M. R.; Merkel, P. B. *J. Am. Chem. Soc.* **1990**, *112*, 3845.

(34) Kovacic, P. *Curr. Med. Chem.: Anti-Cancer Agents* **2005**, *5*, 501.

(35) Manoj, N.; Ajith Kumar, R.; Gopidas, K. R. *J. Photochem. Photobiol., A* **1997**, *109*, 109.

(36) Manoj, N.; Gopidas, K. R. *J. Photochem. Photobiol., A* **1999**, *127*, 31.

(37) Simon, Z.; Balaban, A. T. *Rev. Roum. Chim.* **1964**, *9*, 339.

(38) Wilt, J. R.; Reynolds, G. A.; Van Allan, J. A. *Tetrahedron* **1973**, *29*, 795.

(39) Bigelow, R. W. *J. Chem. Phys.* **1980**, *73*, 3864.

(40) Rulliére, C.; Declemy, A.; Balaban, A. T. *Can. J. Phys.* **1985**, *63*, 191.

(41) Markovitsi, D.; Sigal, H.; Ecoffet, C.; Millie, P.; Charra, F.; Fiorini, C.; Nunzi, J.-M.; Strzelecka, H.; Veber, M.; Jallabert, C. *Chem. Phys.* **1994**, *182*, 69.

(42) Singer, N.; Whittington, P. R.; Boyd, G. V. *Tetrahedron*, **1970**, *26*, 3171.

(43) Boyd, G. V.; Singer, N. *Tetrahedron* **1965**, *21*, 1263.

(44) Parr, R. G. In *Density-Functional Theory of Atoms and Molecules*; Oxford University Press: New York, 1995.

(45) *Modern Density Functional Theory. A Tool for Chemistry*; Seminario, J. M., Politzer, P., Eds.; Elsevier: Amsterdam, 1995.

(46) Becke, A. D. *J. Chem. Phys.* **1993**, *98*, 5648.

(47) Lee, C.; Yang, W.; Parr, R. G. *Phys. Rev.* **1988**, *B37*, 785.

(48) Frisch, M. J.; Trucks, G. W.; Schlegel, H. B.; Scuseria, G. E.; Robb, M. A.; Cheeseman, J. R.; Montgomery, J. A., Jr.; Vreven, T.; Kudin, K. N.; Burant, J. C.; Millam, J. M.; Iyengar, S. S.; Tomasi, J.; Barone, V.; Mennucci, B.; Cossi, M.; Scalmani, G.; Rega, N.; Petersson, G. A.; Nakatsuji, H.; Hada, M.; Ehara, M.; Toyota, K.; Fukuda, R.; Hasegawa, J.; Ishida, M.; Nakajima, T.; Honda, Y.; Kitao, O.; Nakai, H.; Klene, M.; Li, X.; Knox, J. E.; Hratchian, H. P.; Cross, J. B.; Adamo, C.; Jaramillo, J.; Gomperts, R.; Stratmann, R. E.; Yazyev, O.; Austin, A. J.; Cammi, R.; Pomelli, C.; Ochterski, J. W.; Ayala, P. Y.; Morokuma, K.; Voth, G. A.; Salvador, P.; Dannenberg, J. J.; Zakrzewski, V. G.; Dapprich, S.; Daniels, A. D.; Strain, M. C.; Farkas, O.; Malick, D. K.; Rabuck, A. D.; Raghavachari, K.; Foresman, J. B.; Ortiz, J. V.; Cui, Q.; Baboul, A. G.; Clifford, S.; Cioslowski, J.; Stefanov, B. B.; Liu, G.; Liashenko, A.; Piskorz, P.; Komaromi, I.; Martin, R. L.; Fox, D. J.; Keith, T.; Al-Laham, M. A.; Peng, C. Y.; Nanayakkara, A.; Challacombe, M.; Gill, P. M. W.; Johnson, B.; Chen, W.; Wong, M. W.; Gonzalez, C.; Pople, J. A. *Gaussian 03*, version 6.1; Gaussian, Inc.: Pittsburgh, PA, 2003.

(49) Stratmann, R. E.; Scuseria, G. E.; Frisch, M. J. *J. Chem. Phys.* **1998**, 109, 8218.

(50) Bauernschmitt, R.; Ahlrichs, R. *Chem. Phys. Lett.* **1996**, *256*, 454.

(51) Casida, M. E.; Jamorski, C.; Casida, K. C.; Salahub, D. R. *J. Chem. Phys.* **1998**, *108*, 4439.

(52) Zerner, M. C.; Loew, G. H.; Kirchner, R. F.; Mueller, V. T. *J. Am. Chem. Soc.* **1980**, *102*, 589.

(53) Casida, M. E. Time-Dependent Density Functional Response Theory of Molecular Systems: Theory, Computational Methods, and Functionals. In *Recent Developments and Applications of Modern Density Functional Theory*; Seminario, J. M., Ed.; Elsevier: Amsterdam, 1996; p 391.

(54) Bauernschmitt, R.; Ahlrichs, R.; Hennrich, F. H.; Kappes, M. K. *J. Am. Chem. Soc.* **1998**, *120*, 5052.

(55) James, P. V.; Sudeep, P. K.; Suresh, C. H.; Thomas, K. G. *J. Phys. Chem. A* **2006,** *110*, 4329.

(56) Pourtois, G.; Beljonne, D.; Moucheron, C.; Schumm, S.; K-De Mesmaeker, A.; Lazzaroni, R.; Brédas, J.-L. *J. Am. Chem. Soc.* **2004**, *126*, 683.

(57) Cave, R. J.; Burke, K.; Castner, E. W., Jr. *J. Phys. Chem. A* **2002**, *106*, 9294.

(58) Jödicke, J. C.; Lüthi, H. P. *J. Am. Chem. Soc.* **2003**, *125*, 252.